Time-reversal, tori families and canards in the Sprott A and NE9 systems

Taoufik Bakri[1, a)] and Ferdinand Verhulst[1]
Mathematisch Instituut, University of Utrecht, PO Box 80.010, 3508 TA Utrecht, The Netherlands

(*Electronic mail: f.verhulst@uu.nl)

(*Electronic mail: taoufik.bakri@tno.nl)

(Dated: 9 July 2022)

Quadratic 3-dimensional autonomous systems may display complex behaviour. Studying the systems Sprott A and NE9 we find families of tori and periodic solutions both involving canards. Using time-reversal and symmetry we are able to explain in these 2 systems both the analysis and origin of tori, periodic solutions and the numerics of these objects. For system NE9 unbounded solutions exist that admit analytic description by singular perturbation theory of the flow near infinity, also we observe torus destruction and a new chaotic attractor (Kaplan-Yorke dimension 2.1544) produced by a period-doubling scenario. The subtle numerics of periodic solutions involving canards is explained in a final section.

In dissipative systems the presence of an infinite family of tori is unusual. We explain these phenomena for two systems of ODEs, Sprott A and NE9, by showing certain symmetries in the systems. A remarkable additional aspect is that the tori show canard behaviour. Because of the canards the presence of periodic solutions on the tori present special numerical integration problems. There are more surprising phenomena in both simple-looking systems: chaotic behaviour in both systems and in system NE9 an isolated invariant manifold with in its neighbourhood again canard solutions, produced by a stability transition of the manifold.

I. INTRODUCTION

A number of chaotic 3-dimensional systems, in fact 17 autonomous systems with linear and quadratic terms only and one parameter (a), have been listed and studied in[7], see also[15]; all these systems are dissipative, i.e. the 3-dimensional phase-flow is not volume-preserving. The systems are numbered NE1, ..., NE17 with one of them, called Sprott A (or NE1). The study of these 17 systems is very instructive as 3-dimensional systems generally show much more complexity than 2-dimensional ones and as the 17 systems are relatively simple, quadratic and with one parameter. The evidence for chaos in[7] is mainly numerical and an interesting start.
A remarkable aspect of the systems Sprott A and NE9 is the observed presence of families of invariant tori, known in conservative systems but in contrast we have here dissipative systems with the parameter a small. This aspect was studied in more detail for Sprott A in[12] and[13] who correctly observe that we have a kind of KAM tori.

A novel result is that we can complete the theoretical picture both for Sprott A and NE9 by linking the tori bifurcation phenomenon to time-reversal and canards. The scalings near the origin of phase-space in section II and III are related to geometric desingularisation of degenerate singularities. For the vast literature see[8] and[11]. For both systems we can identify a number of periodic solutions on the tori. For the Sprott A system unbounded solutions can only be found on the z-axis. Another novel aspect is that for system NE9 this is different; we find 'rings' of initial values leading to unbounded solutions. Scaling near infinity and using again geometric singular perturbation theory provides insight in this dynamics.

We formulate the equations. The system Sprott A is:

$$\dot{x} = y, \dot{y} = -x - yz, \dot{z} = y^2 - a, \tag{1}$$

with $a \geq 0$. The Sprott A system is a special case of the Nosé-Hoover oscillator; for the physics references of this oscillator and a nice introduction to the theory see[14]. For a number of a values the system (1) suggests chaotic behaviour; if $a \neq 0$ no equilibria exist. In[7] the case $a = 1, x(0) = 0, y(0) = 5, z(0) = 0$ of system (1) produces a structure that looks like an attractor. The 'attracting' object has Kaplan-Yorke dimension 3.0, see[7]. System NE9 shows related but also different characteristics. The equations are:

$$\dot{x} = y, \dot{y} = -x - yz, \dot{z} = -xz + 7x^2 - a, a \geq 0. \tag{2}$$

System NE9 has no equilibrium if $a \neq 0$.

A. Set-up of the paper

In the Introduction we formulate a number of useful lemma's for periodic solutions in the Sprott A and NE9 systems and we observe the time-reversal character of the 2 systems. In section II we consider the Sprott A system adding more details to the canard results of[1] producing for $0 < a \ll 1$ pulse-like behaviour of the solutions. Time-reversal leads to the presence of a tori family around a periodic solution that serves as an organising centre. Infinite families of tori are typical for Hamiltonian systems, see[2]. It is interesting to find such families in dissipative systems. We expect to find periodic solutions on the tori with rather long periods because of

[a)] Also at TNO Sustainable Urban Mobility & safety, PO Box 96800, 2509 JE The Hague, The Netherlands.

their passage through slow manifolds. It takes subtle numerical methods to find the periodic solutions, both stable and unstable (see section V for comments on the numerics). More insight in the presence of tori and the transition to chaos is obtained by using the frequency method of Laskar, see subsection II D.
A striking difference between Sprott A and the NE9 system is the presence of families of unbounded solutions in NE9. The behaviour near infinity requires again singular perturbation analysis and yields insight in the presence of domains where solutions are attracted to infinity. In system NE9 a chaotic attractor with Kaplan-Yorke dimension 2.1544 is detected that emerges from a period doubling sequence. It is demonstrated how periodic solutions, tori and chaos are connected.

B. Some useful observations

Consider systems (1), (2). For arbitrary a the z-axis is an invariant manifold with, if $a \neq 0$, unbounded solutions:

$$x = y = 0, z(t) = z(0) - at. \tag{3}$$

An interesting discrete symmetry feature of (1) is:

Lemma I.1
If $(x(t), y(t), z(t))$ is a solution of system (1) then also $(-x(t), -y(t), z(t))$ is a solution.

This is verified by substitution. An important feature involving time reversal of (1) is:

Lemma I.2
If $(x(t), y(t), z(t))$ is a solution of system (1) then by putting $\bar{x} = x, \bar{y} = -y, \bar{z} = -z$ and reversing time $\tau = -t$, $(\bar{x}(\tau), \bar{y}(\tau), \bar{z}(\tau))$ is also a solution.

Such time-reversal symmetry is called R-symmetry in[9]. For system NE9 we have a similar reversibility as in lemma I.2:

Lemma I.3
If $(x(t), y(t), z(t))$ is a solution of system (2) then by putting $\bar{x} = -x, \bar{y} = y, \bar{z} = -z$ and reversing time $\tau = -t$, $(\bar{x}(\tau), \bar{y}(\tau), \bar{z}(\tau))$ is also a solution.

By differentiating the equation for x we rewrite system (1) as:

$$\ddot{x} + \dot{x}z + x = 0, \dot{z} = \dot{x}^2 - a. \tag{4}$$

Consider the Sprott A system in the form (4). It is easy to prove the following lemma:

Lemma I.4
Assume that $x(t) = \xi(t), y = d\xi/dt, z(t) = \zeta(t)$ are T-periodic ($T > 0$) solutions of system (4) for $a > 0$, then:

$$\int_0^T \zeta(t)dt = 0. \tag{5}$$

Proof
The equation for x with $z = \zeta(t)$ becomes:

$$\ddot{x} + \zeta(t)\dot{x} + x = 0.$$

According to Floquet theory the solutions of the x-equation are of the form $\exp(Bt)\Phi(t)$ with T-periodic matrix $\Phi(t)$ and constant 2×2 matrix B. For the characteristic exponents λ_1, λ_2 we have in the periodic case

$$\lambda_1 + \lambda_2 = \frac{1}{T}\int_0^T \zeta(t)dt = 0,$$

which proves the lemma (the corresponding multipliers ρ_1, ρ_2 satisfy the relation $\rho_1\rho_2 = 1$).

A different proof adds insight to the periodic solutions of system (1).

Alternative proof of lemma I.4
Consider for the solutions of system (4) the function:

$$F(x,y,z) = \frac{1}{2}(x^2 + y^2 + z^2). \tag{6}$$

Differentiation and using the equations yields easily

$$\frac{dF}{dt} = -az,$$

or

$$F(x(t), y(t), z(t)) = F(x(0), y(0), z(0)) - a\int_0^t z(s)ds.$$

If $(x.y.z)$ is T-periodic we have $F(x(0), y(0), z(0)) = F(x(T), y(T), z(T))$ and so, if $a > 0$:

$$\int_0^T z(s)ds = 0.$$

The addional insight is that the quantity $F(x(0), y(0), z(0))$ is conserved with error $O(a)$ on periodic solutions.

It was observed and proved by averaging in[12] that Sprott A system (1) has a periodic solution near the origin of phase-space and for $0 < a \ll 1$. The scaling needed is: $x = \varepsilon\bar{x}, y = \varepsilon\bar{y}, z = \varepsilon\bar{z}, a = \varepsilon^2 a_0$ with a_0 a positive constant. The location is given by $(x(0), y(0), z(0)) = (\sqrt{2a_0}, 0, 0)$. According to[1] the periodic solution exists also for system NE9 with the same scaling; the location for NE9 is given by $(x(0), y(0), z(0)) = (\sqrt{2a_0/7}, 0, 0)$. In both systems the periodic solution is neutrally stable to 2nd order approximation.

Using Poincaré compactification it was shown in[13] for the Sprott A system that the only orbits that can reach infinity are the solutions starting on the z-axis. So all solutions starting outside the z-axis are bounded. The proof does not carry over to system NE9, it is easy to find solutions escaping to infinity numerically.

II. THE SPROTT A SYSTEM

We summarise the degenerate case $a = 0$ studied in[12] as the dynamics for $0 < a \ll 1$ shows very interesting different aspects. We will use the spherical radius R and the distance r to the $z-$axis defined by:

$$R^2 = x^2 + y^2 + z^2,\ r^2 = x^2 + y^2. \tag{7}$$

A. The limit case $a = 0$

It was shown in[12] that for $a = 0$ the behaviour is more regular, in fact integrable. We summarise:

- If $a = 0$, $x = y = z = 0$ is a degenerate critical point of the vector field (equilibrium of the system).
- We differentiate using system (1)

  $$\frac{d}{dt}(R^2) = 2(x\dot{x} + y\dot{y} + z\dot{z}) = -2az.$$

  So if $a = 0$ the spheres with radius R) are invariant manifolds of the system but system (1) is still dissipative.
- If $a = 0$, the z-axis consists of equilibria puncturing the invariant spheres in north- and south-pole. If $0 < R < 2$, the south-pole is an unstable focus, the north-pole a stable focus on each invariant sphere. To see this we differentiate the vector field of system (1):

  $$\begin{pmatrix} 0 & 1 & 0 \\ -1 & -z & -y \\ 0 & 2y & 0 \end{pmatrix}.$$

  If $(x,y,z) = (0,0,\pm R)$, the eigenvalues are on the invariant sphere with radius R: $\frac{1}{2}(R \pm \sqrt{R^2-4})$ (north-pole) and $\frac{1}{2}(+R \pm \sqrt{R^2-4})$ (south-pole). If $R \geq 2$ the 2 pole equilibria are nodes, for $z(0) > 2$ respectively stable and unstable.
  The implication is that for $0 < z(0) < 2$ the solutions near the invariant z-axis are winding towards the axis in the x,y plane, for $-2 < z(0) < 0$ the solutions near the invariant z-axis are winding outwards in the x,y plane with respect to the z-axis.

B. Slow-fast and canard behaviour for a small

Consider now the case $a = \varepsilon$ (a small, positive parameter). We choose the initial values of (x,y,z) in an interior subset D of the sphere with $R = 2$. If $x(0)^2 + y(0)^2 + z(0)^2 < 4$ we keep the rotating character of the flow around the z-axis observed for $a = 0$. It was shown in[1] that if a is small we have a singular perturbation problem with canard behaviour; the behaviour of the solutions for $a = 0$ and $0 < a \ll 1$ is dynamically and topologically very different. We will give the analysis in more detail here, add quantitative aspects and we discuss its geometric consequences.

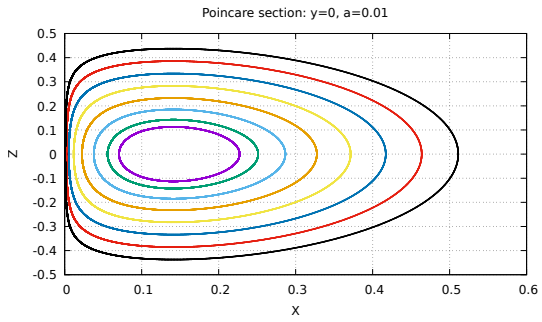

FIG. 1. Poincaré map in the plane $y = 0$ of the Sprott A system (1) near the origin of phase-space for $a = 0.01$. The behaviour near the z-axis shows canard behaviour for various initial conditions.

If a is small it is basic to see system (1) as a slow-fast system and to apply Tikhonov's theorem[16]. Note that

$$\frac{dr^2}{dt} = -\dot{x}^2 z,$$

so, as long as $z(t)$ is positive the (x,y) phase-flow is strongly damped, if $z(t)$ is negative, the flow is excited. When starting with $O(1)$ initial values and $z(0) > 0$, the time needed to produce $x(t), y(t) = O(\sqrt{\varepsilon})$ is $O(|\ln \varepsilon|)$. To put the system in the formulation of Tikhonov's theorem we rescale: $x = \sqrt{\varepsilon}\bar{x}, y = \sqrt{\varepsilon}\bar{y}$. Omitting the bars system (1) becomes:

$$\dot{x} = y,\ \dot{y} = -x - yz,\ \dot{z} = \varepsilon(y^2 - 1), \tag{8}$$

and rescaling time $\tau = \varepsilon t$ we find the equivalent system:

$$\varepsilon \frac{dx}{d\tau} = y,\ \varepsilon \frac{dy}{d\tau} = -x - yz,\ \frac{dz}{d\tau} = y^2 - 1. \tag{9}$$

According to geometric singular perturbation theory system (8) shows fast motion of the x,y-component except in an $O(\varepsilon)$ neighbourhood of the 1-dimensional slow (or critical) manifold M_0 defined by:

$$y = 0,\ -x - yz = 0. \tag{10}$$

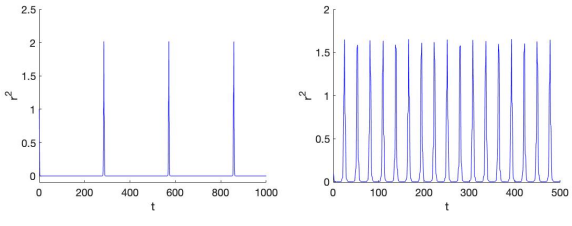

FIG. 2. Pulses of $r^2(t)$ showing the fast motion of the (x,y)-flow with respect to the z-axis that is near the slow manifold. Left we have $a = 0.01, x(0) = 1, y(0) = 0, z(0) = 1$, right $a = 0.1, x(0) = 0.3162, y(0) = 0, z(0) = 1$. The behaviour near the z-axis shows canard behaviour.

The slow manifold M_0 corresponds with the z-axis in 3-dimensional phase-space, it is normally hyperbolic when excluding a neighbourhood of $z=0$ as we have for the fast part of the system that the real part of the spectrum is $-z/2$. M_0 approximates the smooth slow manifold M_ε that exists for solutions of system (8). According to section 15.7 of[18], when excluding a neighbourhood of $z=0$, M_0 approximates M_ε exponentially close. To fix ideas we take initially

$$x(0)=x_0, y(0)=0, z(0)=z_0, 0<x_0, z_0<2.$$

We assume that x_0, z_0 are not ε-close to 0 or 2. According to Tikhonov we have when starting outside M_0 at positive $z(0)=z_0$ an $O(\varepsilon)$ approximation of the fast solutions of system (8) of the form:

$$X_0(t)=x_0 e^{-z_0 t/2}\cos(\sqrt{4-z_0^2}\,\frac{t}{2}). \tag{11}$$

The approximation is valid on an interval $O(1)$ in τ, $O(1/\varepsilon)$ in t as long as we do not enter a ε-neighbourhood of M_0. From (11) we can estimate the fast time T_1 needed to approach M_0:

$$x_0 e^{-z_0 T_1/2}\cos(\sqrt{4-z_0^2}\,\frac{T_1}{2})=\varepsilon. \tag{12}$$

Ignoring the oscillations a rough estimate is

$$T_1 \leq -\frac{2}{z_0}\ln\left(\frac{\varepsilon}{x_0}\right). \tag{13}$$

The approximate time needed for the motion until $z=0$ along M_0 is $T_2=z_0/\varepsilon$. Using the symmetry result of lemma I.2 we find the estimate of the return time $T\geq 2(T_1+T_2)$ of the flow in system (8). The pulse-like behaviour for the fast motion of the flow is shown in fig. 2. The slow-fast system (8) is actually valid in an $O(\sqrt{\varepsilon})$ neighbourhood of the origin whereas in fig. 2 we start the solutions outside this region; this is possible because of the strong damping if $z(t)>0$ but it will produce a lower bound of the return time.

Geometric singular perturbation theory in combination with time reversal and symmetry produces the behaviour shown in the Poincaré maps of fig. 1. Increasing ε we expect the tori to break up, maybe with Cantor gaps as in near-integrable Hamiltonian systems.

C. Tori and periodic solutions for small a

In this subsection periodic orbits will be described obtained by the procedure outlined in section V.
It has become clear that lemma I.2 regarding time reversal and symmetry plays an essential part in producing recurrence of the canards and tori-like structures. As we will show in subsection II E unfolding system (1) destroys the reversal symmetry and the tori-like structures. Time-reversal symmetry plays a part in what is sometimes called "dissipative KAM theory", see for surveys[14,3,9].
For the Sprott A system this was conjectured in[12] and[13] with strong numerical evidence. There exist a large number of papers describing the emergence of quasi-periodic solutions and tori near equilibria with purely imaginary eigenvalues, sometimes in 3-space with a zero eigenvalue added. However, the framework for the Sprott A system is different as for a (or ε) zero we have an infinite set of equilibria whereas for $a>0$ we have no equilibrium in the system, the infinite set persists as invariant manifold of the system. For $a=0$ phase-space is foliated into invariant spheres that collapse to tori for $0<a\ll 1$. In our analysis we have a periodic solution at $O(\varepsilon)$ distance of 3-dimensional phase-space. This periodic solution is surrounded by the infinite set of slow-fast solutions we derived in subsection II B. This follows from the estimates in section 15.7 of[18], when excluding a neighbourhood of $z=0$ and the time-reversal characteristic.

It makes sense to have a closer look at the tori. First we note that the theory of canards guarantees the presence of slow manifolds for a small enough. The slow manifolds are tunneling exponentially close to the z-axis parametrised by $z(0)$. The reversibility result of lemma I.2 yieds a tori family of which the dynamics still has to be explored.

It is interesting to look for periodic solutions embedded in tori by using lemma I.4. Define

$$I(t)=\int_0^t z(s)ds.$$

Look for T-periodic zeros of $I(t)$, maybe varying ε for fixed z_0; T will be close to the return times of the tori.
It might help to consider maps of the x,I-plane into itself for $y=0$. These maps will be used to find periodic solutions numerically later on.

It was shown in[12] and[13] and to 2nd order in[1] that on scaling $x,y,z=O(\varepsilon)$ and $a=\varepsilon^2 a_0$ a Lyapunov stable periodic solution exists $O(\varepsilon^2)$-close to the invariant manifold $z=0$ and the circle $x^2+y^2=2a_0\varepsilon^2$. As a_0 is an arbitrary $O(1)$ constant this means that we have found a family of periodic solutions that gives for each fixed a an *organising centre* of the family of tori. An example of this family is periodic orbit 2 of table I.

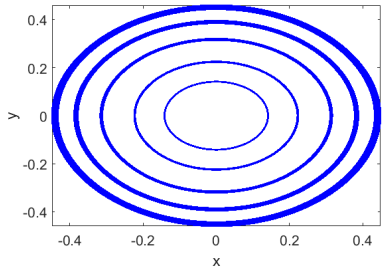

FIG. 3. Five orbits in tori and $O(\varepsilon^2)$-close to 5 members of the family of periodic solutions in the Sprott A system (1) with projection in the (x,y) plane given by $x^2+y^2=2a$. We took successively $a=0.1, 0.075, 0.05, 0.025, 0.01$ corresponding to $y(0)=0, z(0)=0.00575, 0.003, 0.0018, 0.0009, 0.00001$.

A different periodic solution is shown in fig. 4. This periodic solution of system (1) in a torus near the origin is

found by numerical bifurcation analysis for $a = 0.013149$; $x(0) = -0.0985, y(0) = 0.09811, z(0) = 0.9951$. The slow manifold shows up in the centre of the (x,y) projection (left figure) and in the vertical z motion in the (x,z) projection (middle); the observed asymmetry in the (x,y) projection gives us the mirrored periodic solution (right in figure) guaranteed by lemma I.1. For the 3 Lyapunov exponents of this periodic solution we find zero.

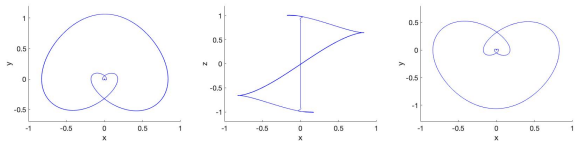

FIG. 4. Periodic solution of system (1) in a torus near the origin of phase-space for $a = 0.013149$; $x(0) = -0.0985, y(0) = 0.09811, z(0) = 0.9951$. The vertical motion in the x,z projection (middle) corresponds with the slow manifold. Right the corresponding mirrored periodic solution with $a = 0.013149$; $x(0) = 0.0985, y(0) = -0.09811, z(0) = 0.9951$.

Numerical integrations show that the recurrence of the orbits in the tori is generally not periodic, but we can find more isolated, stable periodic solutions; see again table I. We have strong dependence of the tori on the initial conditions $(x(0), y(0)) = O(\sqrt{\varepsilon})$ and $z(0)$.

Orbit	x(0)	y(0)	z(0)	Comment
1	1.8695994059332728	0.2944520589918199	0.0110866612202986	symm?
2	0.4291037205668491	0.0987225690750841	0.0218388331274574	symm?
3	0.4744357151957521	0.0983426673450300	0.8576750212812009	asymm
4	0.2774893842985010	0.0995749781953782	-1.3419264311707517	asymm
5	2.3540732574727441	0.0930243663640321	0.0038354394368108	asymm
6	1.7908932567444744	0.0014155008257577	0.0000790590874794	asymm
7	1.3437830881665427	-0.0049654722303571	-0.0003694822052058	asymm
8	1.2257230457685124	-0.0079551776672382	-0.0006488696242273	symm ?
9	1.4671282026917492	-0.0004444199767620	-0.0000302875267243	symm ?
10	2.2333901966540153	-0.0066173642003448	-0.0002962481436574	asymm
11	1.7428203499839363	-0.0051638432948303	-0.0002962650562144	asymm

TABLE I. Initial values of 11 periodic orbits with $a = 0.1$. According to lemma I.1 the 7 asymmetric orbits (asymm) yield additional periodic orbits by the symmetry $-x(t), -y(t), z(t)$. In the cases of orbits 1, 2, 8, 9 with 'symm ?' in the last column the orbits are looking symmetric in the (x,y) projection but a proof is lacking.

The periodic orbits of table I

The Poincaré maps of the periodic orbits show collections of segments that consist of isolated points that correspond with the transitions of the transversal plane of section. Segments arise because of the slow-fast dynamics of the orbits if a is small.

The exception is orbit 2 that is part of the family that forms the organising centre of the tori. For orbit 2 in this family the Poincaré section is a fixed point, the (x,y) projection is close to a circle.

As mentioned in the caption of table I at least 7 additional periodic orbits exist because of symmetry considerations. In fig. 5 we present a few typical examples of table I. Orbit 8 looks rather complex; we illustrate its behaviour with time in fig. 6

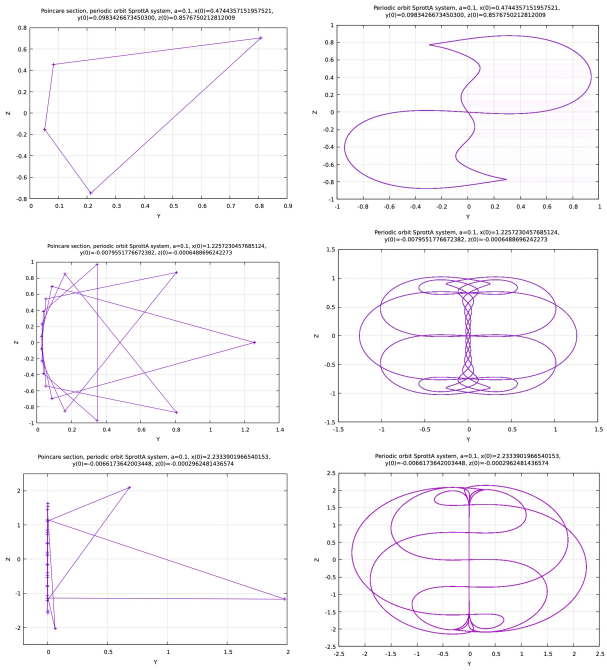

FIG. 5. Periodic solutions of system (1) from table I. Succesively the orbits 3 (asymmetric but simple), 8 and 10 (more complex orbits). Left the Poincaré sections consisting of many points, right the projections on the (x,y) plane.

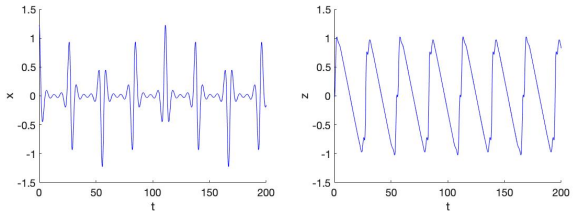

FIG. 6. Timeseries $x(t)$ and $z(t)$ ot orbit 8 in table I. .

for $x(t), z(t)$. In accordance with lemma 5 we find for the z,I-diagram ($I = \int_0^t z(s)ds$) a closed loop (picture not shown).

The stability of the periodic solutions follows from the 3 Lyapunov multipliers. As the Sprott A system is autonomous one multiplier ρ_1 will always be 1; lemma I.4 and the time reversality yields that for the 2 remaining multipliers we have $\rho_2 = 1/\rho_3$; see table II. We have stability if $|\rho_i| = 1, i = 1,2,3$.

To find unstable periodic orbits is more difficult. We list 5 unstable cases in table III. The Poincaré sections and projections on the (x,y) plane are shown in fig. 7

The R-symmetric orbits of table I have all their complex multipliers on the unit circle, the orbits are Lyapunov stable. It is important to note that there exist also periodic orbits with real multipliers outside the unit circle in the complex plane, they are unstable; see tables III and IV.

Orbit	Period	Multipliers ρ_1, ρ_2, ρ_3
1	80.35	1; 0.0576 + 0.99839i; 0.0576 - 0.9983i
2	6.21	1; -0.3702 + 0.9289i; -0.3702 - 0.9289i
3	25.80	1; 0.9822 + 0.1878i; 0.9822 - 0.1878i
4	34.40	1; 0.8610 + 0.5086i; 0.8610 - 0.5086i
5	98.53	1; 0.5801 + 0.8145i; 0.5801 - 0.8145i
6	1.15	1; 0.9878 + 0.1560i; 0.9878 - 0.1560i
7	59.69	1; 0.7648 + 0.6443i; 0.7648 - 0.6443i;
8	111.19	1; 0.9952 + 0.0974i; 0.9952 - 0.0974i
9	128.46	1; 0.9713 + 0.2379i; 0.9713 - 0.2379i
11	149.48	1; 0.9158 + 0.401i; 0.9158 - 0.401i

TABLE II. Periods and multipliers of 11 stable periodic orbits of table I (system (1)). Of the 16 decimals we show for the periods 2 decimals for the multipliers 4. In each case $|\rho_i| = 1$, $i = 1,2,3$.

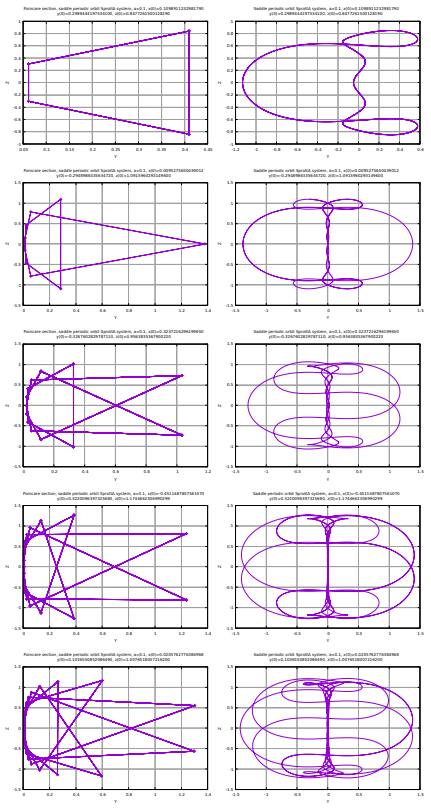

FIG. 7. Five unstable periodic solutions of system (1) from table III. Left the Poincaré sections consisting of many points, right the projections on the (x,y) plane.

D. Fundamental frequencies in the chaotic regions

The method of fundamental frequencies was first introduced by Laskar in 1990 where he used it to estimate the size of the chaotic zones in a 15 degrees of freedom dynamical system. The idea behind it is that the frequency map is still exactly defined on the Cantor set of the invariant tori. It can be thought of as a diffeomorphism on this set. Chaotic zones will therefore appear as loss of regularity regions for the frequency map. This approach is more accurate than using Lyapunov exponents and computing the Kaplan-Yorke dimension as the frequency variations directly signal the break-up of invariant tori. This criterion is used here to identify chaotic behavior in the SprottA system. The fundamental frequencies were computed using the SDDS NAFF algorithm by Laskar, see[10] for more details on the approach of numerical analysis of the frequencies (NAFF).

Orbit	x(0)	y(0)	z(0)	Comment
1B	0.1098911232981790	0.2989444197534100	0.8477261500128190	asymm
2B	0.0095275650439012	-0.2948986335634720	1.0915960293149600	symm ?
3B	0.3237216296199650	-0.3267602829787110	0.9563835367900220	asymm
4B	-0.4511487807561070	0.3220096397325680	1.1744662306990299	symm ?
5B	0.0205762776384968	0.1036550852086490	1.0076518007216200	asymm

TABLE III. Initial values of 5 periodic orbits with $a = 0.1$. According to lemma I.1 the 3 asymmetric orbits (asymm) correspond with a periodic orbit $-x(t), -y(t), z(t)$. In the cases of orbits 2B,4B the orbits are looking symmetric in the $x,y)$ projection but a proof is lacking.

Orbit	Period	Multipliers ρ_1, ρ_2, ρ_3
1B	25.82	1; 0.8278; 1.2080
2B	59.85	1; 0.4951; 2.01977
3B	85.44	1; 0.9858; 1.0144
4B	128.46	1; 0.7867; 1.2711
5B	307.59	1; 0.9779 1.0226

TABLE IV. Periods and multipliers of 5 unstable periodic orbits of table III (system (1)). Of the 16 decimals we show for the periods 2 decimals for the multipliers 4.

In fig. 8 we show the fundamental frequencies as a function of $x(0)$ in the tori and chaotic regions for $a = 0.1$. Left in fig. 8 we run $x(0)$ from 0 to 0.13 showing a clear and regular pattern. Right in the figure we have zoomed in near the origin $(-0.0004 < x(0) < +0.0004)$; near $x(0) = 0$ we have an accumulation of frequencies and loss of regularity of the frequency map yielding therefore chaotic motion in the SprottA system at parameter value $a = 0.1$.

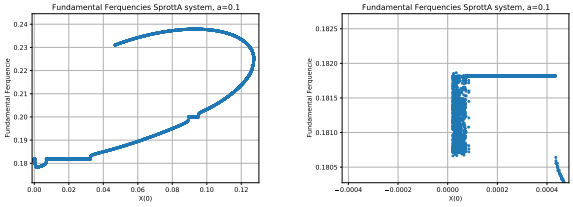

FIG. 8. The frequencies in the neighbourhood of the origin in the tori and in the regions between them.

E. Unfolding near eigenvalue zero

The time reversality is essential for our results; we show this by unfolding of the singularity and breaking time reversality. If $a = 0$ we have a zero eigenvalue for the critical point

at the origin. We propose the following unfolding using positive parameter c:

$$\dot{x} = y, \dot{y} = -x - yz, \dot{z} = y^2 - a - cz. \tag{14}$$

Lemma I.2 does not hold anymore, the time symmetry is broken. The z-axis is still an invariant manifold; starting at $(x,y,z) = (0,0,z_0)$ the solution is:

$$z(t) = -\frac{a}{c} + (z_0 + \frac{a}{c})e^{-ct}. \tag{15}$$

If $a = 0, c > 0$, the origin is a stable focus with 1 negative eigenvalue and 2 purely imaginary ones. The spheres $R^2 = x^2 + y^2 + z^2 =$ constant are no longer invariant manifolds; $dR^2/dt = -2cz^2$.
If $a > 0, c > 0$, we have on the negative z-axis the critical point $(x,y,z) = (0,0,-a/c)$; if a is fixed and c tends to zero, this critical point moves to minus infinity and is stable. We will characterise the dynamics near the invariant z-axis in the case $0 < a, c \ll 1$.
In eq. (14) we rescale $x = \sqrt{\varepsilon}\bar{x}, y = \sqrt{\varepsilon}\bar{y}, a = \varepsilon a_0, c = \varepsilon c_0$; omitting the bars we obtain:

$$\dot{x} = y, \dot{y} = -x - yz, \dot{z} = \varepsilon y^2 - \varepsilon a_0 - \varepsilon c_0 z. \tag{16}$$

This is a slow-fast system with again slow manifold $x = y = 0$, the slow manifold is hyperbolic unless $z = 0$. If $z(0) > 0$ the (x,y) oscillations are strongly damped and the phase-flow moves to the z-axis. The Tikhonov theorem[16] can be used as in the case $c = 0$. We find again recurrent canard behaviour but not the presence of invariant tori as it turns out that the solutions tend for $0 < a, c \ll 1$ to a stable periodic solution near the origin. We show this using a different scaling of eq. (14): $x = \varepsilon\bar{x}, y = \varepsilon\bar{y}, z = \varepsilon\bar{z}, a = \varepsilon^2 a_0, c = \varepsilon c_0$; omitting the bars we obtain:

$$\dot{x} = y, \dot{y} = -x - \varepsilon yz, \dot{z} = \varepsilon y^2 - \varepsilon a_0 - \varepsilon c_0 z. \tag{17}$$

Using transformation to cylindrical coordinates:

$$x = r\cos(t+\psi), y = \dot{x} = -r\sin(t+\psi), z = z, \tag{18}$$

we find the variational system:

$$\begin{cases} \dot{r} &= -\varepsilon r \sin^2(t+\psi)z, \\ \dot{\psi} &= -\frac{1}{2}\varepsilon \ \sin(2t+2\psi)z, \\ \dot{z} &= \varepsilon r^2 \sin^2(t+\psi) - \varepsilon(a_0 - c_0 z). \end{cases} \tag{19}$$

Averaging to first order produces equations governing the approximations for r, ψ, z:

$$\dot{r} = -\frac{\varepsilon}{2} rz, \ \dot{\psi} = 0, \dot{z} = \frac{\varepsilon}{2}(r^2 - 2a_0 - 2c_0 z). \tag{20}$$

If $r_= \sqrt{(2a_0)}, z = 0$, we have an equilibrium of the averaged system (20). According to theorem 11.5 in[17] (so-called 2nd Bogoliubov theorem) the autonomous system (17) has a periodic solution in an $O(\varepsilon)$ neighbourhood of the equilibrium if the $n \times n$ Jacobian matrix at this point has rank $n-1$; this is the case here. We find 2 complex eigenvalues and 1 negative eigenvalue $O(\varepsilon)$, so an isolated stable periodic solution exists in an $O(\varepsilon)$ neighbourhood of the origin.The behaviour of the Sprott A system unfolded near the origin is similar to the behaviour of system NE8, see for details[1].

III. SYSTEM NE9 FOR PARAMETER a SMALL

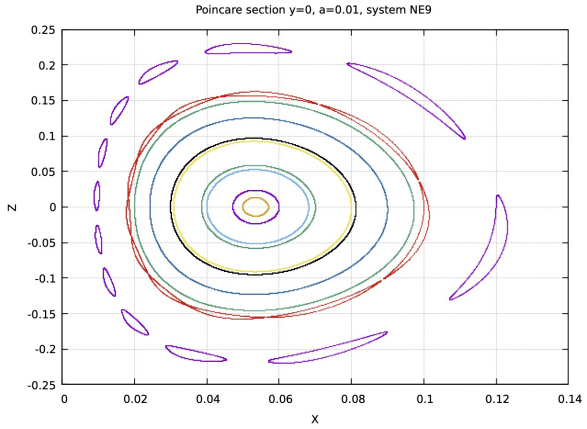

FIG. 9. Poincaré map in the plane $y = 0$ of system (2) near the origin of phase-space for $a = 0.01$. The numerics shows tori near the origin of phase-space as in the Sprott A system..

The analysis of Sprott A system (NE1) for a small carries partly over to system NE9 as similar time-reversal plays a part but there are interesting new aspects like the presence of sets of unbounded solutions, tori destruction and a new chaotic set.
If $a = 0$ the origin of phase-space is an equilibrium with eigenvalues $\pm i, 0$. The first 2 equations of system (2) are the same as for the Sprott A system, the implication is that also in system NE9 the (x,y) flow is strongly damped as long as $z(t) > 0$. See fig. 9 for the tori that emerge near the origin of phase-space and a small; this region near the origin is smaller than in the case of the Sprott A system.
The behaviour of the canards and the corresponding pulses are quantitatively different from the Sprott A system, see fig. 10

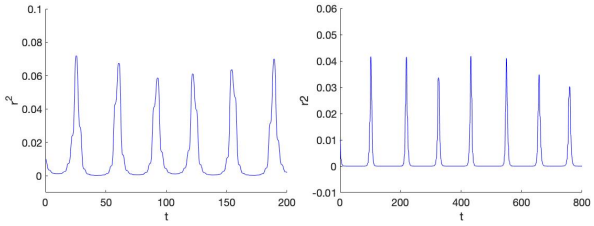

FIG. 10. Pulses of $r^2(t)$ showing the fast motion of the (x,y)-flow with respect to time including the slow manifold for system (2), NE9. Left we have $a = 0.05, x(0) = 0.1, y(0) = 0, z(0) = 0.4$, right the same initial conditions but $a = 0.01$. The behaviour near the z-axis shows canard behaviour but for $a = 0.01$ the pulses are more irregular.

A. Tori and periodic solutions for small a

As in subsection II C the numerical analysis of periodic solutions in system NE9 refers to section V.

We rescale $x, y, z = O(\varepsilon)$ and $a = \varepsilon^2 a_0$. It was shown in[1] that a Lyapunov stable periodic solution exists $O(\varepsilon^2)$-close to the invariant manifold $z = 0$ and the circle $x^2 + y^2 = \frac{2}{7} a_0 \varepsilon^2$. As a_0 is an arbitrary $O(1)$ constant this means that we have found again a family of periodic solutions that we expect to produce for fixed a an *organising centre* of a family of tori. Lemma I.3) guarantees time reversal and symmetry.

To analyse the canards we use a different scaling. Again we put $a = \varepsilon$ with small parameter $\varepsilon \geq 0$. As in section II we put the system in the formulation of Tikhonov's theorem, here by rescaling $x = \varepsilon \bar{x}, y = \varepsilon \bar{y}$. Omitting the bars system (2) becomes:

$$\dot{x} = y, \dot{y} = -x - yz, \dot{z} = \varepsilon(-xz + 7\varepsilon x^2 - 1), \qquad (21)$$

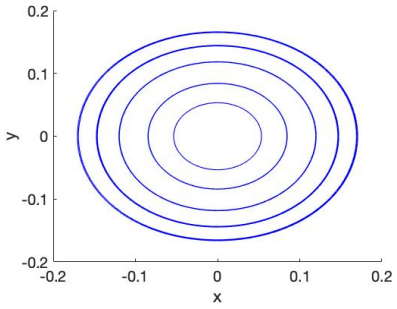

FIG. 11. Five orbits in tori and $O(\varepsilon^2)$-close to 5 members of the family of periodic solutions in the NE9 system (2) with projection in the (x, y) plane given by $x^2 + y^2 = \frac{7}{2} a$. We took successively $a = 0.1, 0.075, 0.05, 0.025, 0.01$.

The slow manifold M_0 corresponds as before with the z-axis in 3-dimensional phase-space, it is normally hyperbolic when excluding a neighbourhood of $z = 0$. M_0 approximates the smooth slow manifold M_ε that exists for solutions of system (21) exponentially close when excluding a neighbourhood of $z = 0$ (see again section 15.7 of[18]). As for system NE1 the family of canard solutions surround the small family of periodic solutions near the origin as in subsection I B.
From the canard behaviour we have via time reversal and symmetry (lemma I.3) the emergence of tori for parameter a small. However, the pulses for system NE9 in fig. 10 show more variation than in the NE1 case. These variations are caused by the different terms in the z-equation.
In fig. 12 we show a few examples of periodic solutions.

IV. SYSTEM NE9, BOUNDEDNESS AND CHAOS

System NE9 has many other interesting features if we admit larger values of the parameter a. We will discuss boundednes of solutions and explore for $O(1)$ values of parameter a the presence of tori and strange attractors.

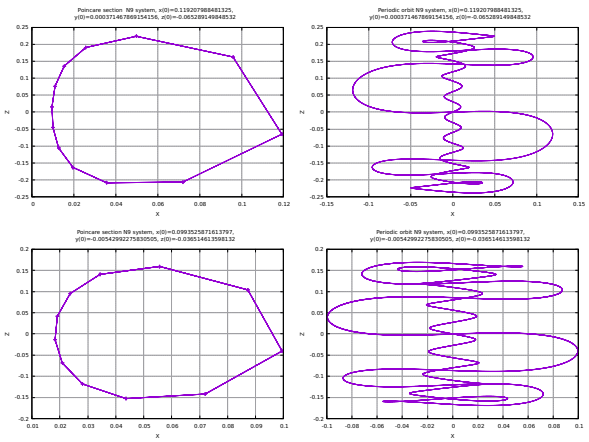

FIG. 12. We show a R-symmetric periodic stable solution of system NE9, $a = 0.01$ (top position). Multipliers [0.999999999510044 ;0.901390727296870 + 0.433006647792041i;0.901390727296870 - 0.433006647792041i]. Left the Poincaré section and right the projection on the (x, z)-plane, period: 69.3070. Below an unstable solution, period 75.7092. Multipliers [0.999999999630394; 0.992154675576315 + 0.125016399303422i; 0.992154675576315 − 0.125016399303422i, located on the unit circle. Left the Poincaré section, right the projection on the (x, z)-plane.

.

A. Bounded and unbounded solutions

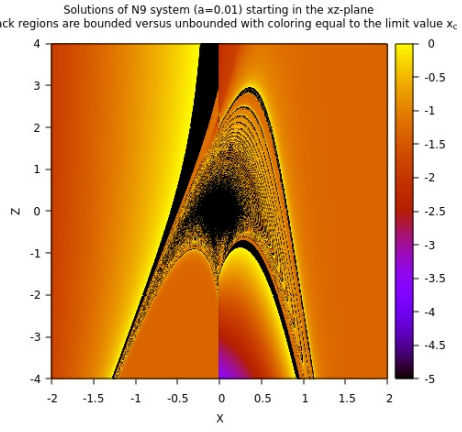

FIG. 13. The solutions of system NE9, $a = 0.01$ that become unbounded start in the coloured regions of the (x, z)-plane, the limiting value x_c is indicated by the colour; the black regions correspond with bounded solutions. Left initial conditions starting at $-2 < x < 2, -4 < z < 4$, right a zooming in at the upper corner.

Consider again system NE9 (2) but now regarding boundedness of the solutions. In fig. 13 we present regions of initial conditions (yellow) that produce unbounded solutions if $a = 0.01$; the black regions correspond with initial conditions for bounded solutions. We repeat the search for bounded and

unbounded solutions for $a- = 0.55$, see the results in fig. 14.

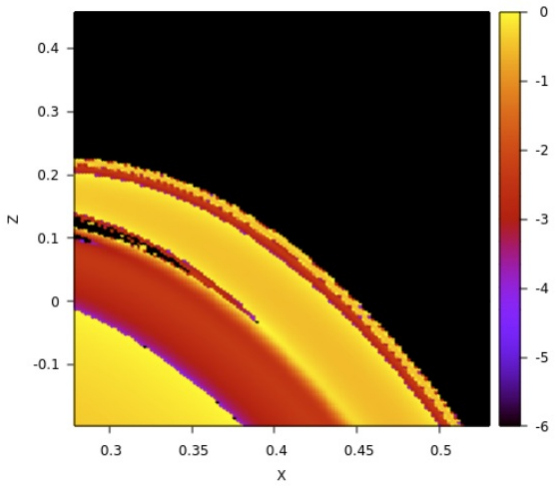

FIG. 14. The solutions of system NE9, $a = 0.55$ that become unbounded start in the coloured regions of the (x,z)-plane, the limiting value x_c is indicated by the colour; the black regions correspond with bounded solutions.

The numerics shows that $z(t)$ becomes unbounded, $y(t)$ tends in this case to zero whereas $x(t)$ tends to a fixed number, dependent on the initial conditions, see fig. 13. Using this information we give arguments for the behaviour near infinity by transforming $z = 1/w$; system (2) becomes:

$$\dot{x} = y, \dot{y} = -x - \frac{y}{w}, \dot{w} = xw - 7x^2w^2 + aw^2, a \geq 0. \quad (22)$$

We have that $w = 0$ is a solution if $y(t)$ tends to zero and faster than $w(t)$; another condition will be that for certain t_0 and $t \geq t_0$, we have $x(t) < 0$. Suppose that $w(t) \neq 0$ but $O(\varepsilon)$. We rescale $w = \varepsilon\bar{w}$, system (22) can be written as:

$$\dot{x} = y, \varepsilon\dot{y} = -\varepsilon x - \frac{y}{\bar{w}}, \dot{\bar{w}} = x\bar{w} - \varepsilon 7x^2\bar{w}^2 + \varepsilon a\bar{w}^2, a \geq 0. \quad (23)$$

According to singular perturbation theory, see[18], $y(t), t \geq t_0$ moves to zero in a fast fiber if $w(t_0) > 0$ with timelike variable t/ε, $\bar{w}$ tends to zero with timelike variable t. This shows that $w = 0$, with the assumptions given above, corresponds with a set of solutions of system (22); we have for this set $y(t) \to 0$ and $x(t)$ tends to $x_c = x(t_0) + O(\varepsilon)$. The computation gives also a hint regarding the origin of the structure of 'rings' of initial conditions leading to bounded and unbounded solutions. We noted that for $w = (1/z) = 0$ to be an attractor we have the condition $x(t) < 0, t \geq t_0$. We expect that for various starting values of $x(t)$ this component of the system will still oscillate before it enters the neighbourhood of $w = 0$ for $t \geq t_0$. Its sign at $t = t_0$ will determine the final boundedness. As qualitative arguments this reasoning is sound but note that the analysis of the quantitative behaviour is for a large part numerical.

The case $a = 1$

A special unbounded solution arises if $a = 1$. We find on the manifold $z = 7x$ the solutions:

$$x(t) = -\frac{t}{7} + x(0), y = -\frac{1}{7}, z(t) = -t + 7x(0). \quad (24)$$

The family of solutions is parameterised by $x(0)$, the sign of $x(0)$ is for $a = 1$ clearly not important. Linearisation of system (2) for $a = 1$ at this special solution produces structural stability of the solution when a neighbourhood of $x = 0$ is excluded. The solution is asymptotically stable if $x > 0$ and unstable if $x < 0$. The structural stability implies continuation for a finite interval of time when excluding a neighbourhood of $x = 0$. This agrees with the picture of fig. 16 where $a = 0.99$.The solution for $a = 0.99$ follows the set $z = 7x$ and shows canard behaviour when passing the region where $x = 0$. We transform $x, y, z \mapsto x, v, w$ by:

$$x = x, y = y, w = z - 7x. \quad (25)$$

We find the system satisfying $w = 0, a = 1$:

$$\dot{x} = y, \ \dot{y} = -x - yw - 7xy, \ \dot{w} = -xw - 7y - a. \quad (26)$$

In fig. 15 the bounded solutions are shown in yellow regions of the x,z-diagram for $a = 1$ and $a = 0.99$ Choosing a close to

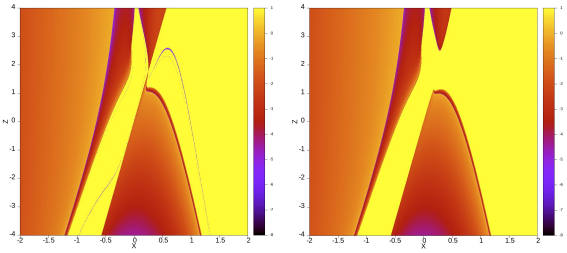

FIG. 15. Left the bounded solutions indicated by yellow regions in the x,z-plane of system NE9 with $a = 1$; the solutions start at $y(0) = -1/7$.The manifold $z = 7x$ shows up, the nearby behaviour looks complex. Right the case $a = 0.99$, again starting at $y(0) = -1/7$.

1, say $a = 1 - \varepsilon$,the structural stability of the exact solution enables us to approximate $w(t)$ as long as we do not enter a neighbourhood of $x = 0$. We have no need for the usual slow manifold scaling. We find with exact solution (24) for the equation with approximate $w(t)$:

$$\dot{w} = -(x(0) - \frac{t}{7})w + \varepsilon, w(0) = 0. \quad (27)$$

The approximate solution is:

$$w(t) = \varepsilon e^{(-x(0)t + \frac{t^2}{14})} \int_0^t e^{(x(0)s - \frac{s^2}{14})} ds, 0 \leq t \leq 7x(0).$$

The term $t^2/14$ dominates the expression with consequence that the canard behaviour, following the manifold $z = 7x$ where it has become unstable, depends with $O(\varepsilon)$ on $x(0)$.

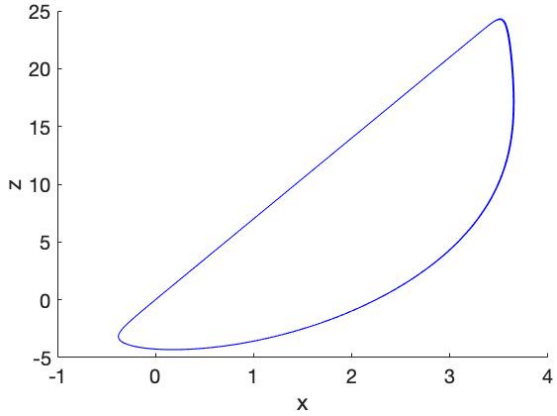

FIG. 16. Solutions in the x,z-plane of system NE9 with $a = 0.99$; the solutions start at $z(0) = 7x(0), y(0) = -1/7$ for $x(0) = 0.5, 2, 3$, they can hardly be distinguished.

This is confirmed by the numerics of the system, see fig. 16. We find a family of periodic solutions with canard behaviour as the slow manifold $z = 7x$ is followed for some time where it is unstable, but as $w(7x(0)) = O(\varepsilon)$ the solutions are very close (in fig. 16 $\varepsilon = 1 - a = 0.01$).

Bifurcation analysis of the periodic orbit near the canard

Continuation of the periodic orbit at $a = 0.99$ with respect to the parameter a yields the following bifurcation diagram. Continuation of the periodic solution with respect to the parameter a and starting at $a = 0.99$ yields twice a period doubling. The first one occurs at $a = 5.75379 \times 10^{-1}$ where the orbit undergoes a supercritical period doubling bifurcation with normal form coefficient $l_1 = -4.893206 \times 10^{-5}$ and period $T = 8.24$) , becomes unstable and a stable period 2 orbit bifurcates from it. The unstable periodic period 1 orbit undergoes a second supercritical period doubling bifurcation with Normal form coefficient $l_1 - 6.610245 \times 10^{-3}$) and period $T = 6.93$ at the parameter value $a = 4.65681 \times 10^{-1}$. The other two period doubling are related to the first two by the symmetry in the NE9 system. At $a = 4.11888 \times 10^{-1}$ a fold bifurcation occurs where the time-reversal symmetrically related orbits collide in a symmetric orbit and disappear. See fig. 18.

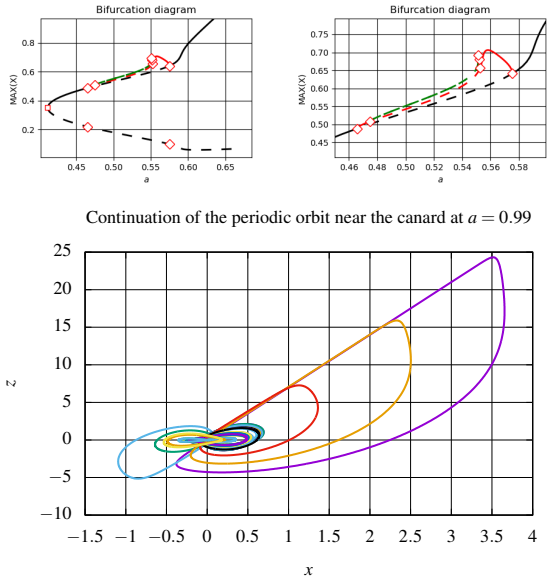

FIG. 17. Bifurcation diagram of the periodic orbit near the canard solution. The diamond symbol (upper figure) correspond with Period doubling bifurcations. The square symbol indicates a fold bifurcation. Dashed lines mean the periodic orbit is unstable.

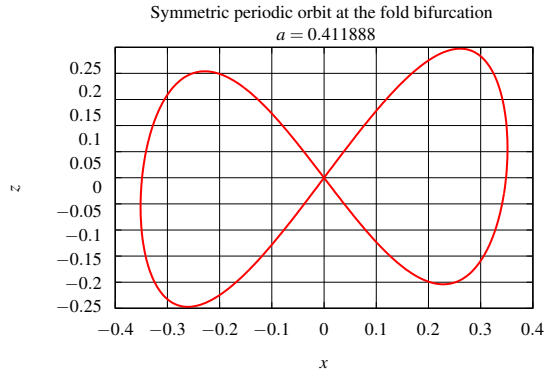

FIG. 18. Time-reversal symmetrically related orbits collide in a symmetric orbit and disappear

B. Tori and chaos for NE9

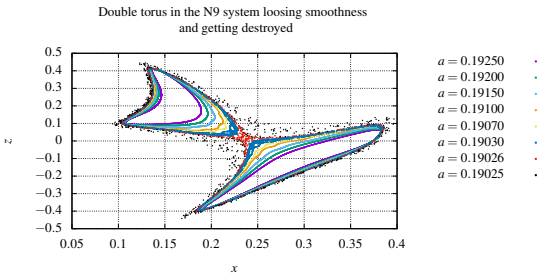

FIG. 19. Projection of a torus on the x,z-plane in system NE9, $a \approx 0.19$. Varying a it gets into a state of non-smoothness and then becomes a double torus.

The presence of periodic solutions and tori was demonstrated for small values of a in section III A. Interestingly destruction of tori can be observed when decreasing the parameter a. Decreasing from $a = 0.1925$ until $a = 0.19026$ we observe the changes of a double torus that is loosing smoothness, collapsing on itself and getting destroyed at some point; see fig. 19. In[7] a chaotic set is identified for $a = 0.55, x(0) =$

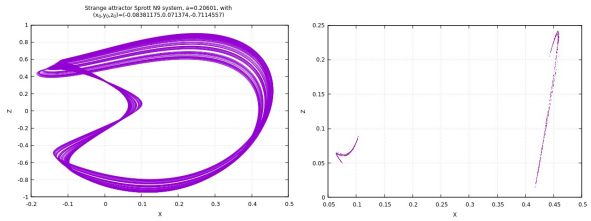

FIG. 20. Left the projection of a chaotic attractor on the x,z-plane in system NE9, $a = 0.20601$, initial values $(x,y,z)(0) = -0.08311175, 0.071374, -0.7114557$. Right the Poincaré section of the attractor transversing the plane $y = 0$.

$0.5, y(0) = z(0) = 0$, Kaplan-Yorke dimension $D_{KY} = 2.1544$. One can identify more chaotic sets, see fig. 20 for the case $a = 0.20601$, the attractor is reminiscent of a full torus perforated an infinite number of times. It is important to understand its origin by analysing the corresponding chaotic scenario. It turns out that by continuation of certain periodic solutions a cascade of period doublings produces a chaotic attractor. This is the case when starting for instance with the periodic solution found by averaging, see the start of subsection III A. plaats vindt. The period doublings of periodic orbits $P_i, i = 1,\ldots,5$ for several values of a are shown in table V. The ratio's $(a(P_{i+1}) - a(P_i))/(a(P_{i+2}) - a(P_{i+1}), i = 1,2,3$ are

Orbit	Value a
P1	0.203744391
P2	0.205393369
P3	0.205695124
P4	0.205758533
P5	0.205772131

TABLE V. Period doublings and corresponding values of a in system NE9..

$5.46463, 4.75887, 4.66311$ and tend to the Feigenbaum constant $\delta = 4.6692$. In fig. 21 we show the cascade of period doubling starting with a periodic R-asymmetric orbit.

Another way to display the chaotic attractor of fig. 20 is showing it in 3-space, see fig. 22.

V. NUMERICAL COMPUTATION OF PERIODIC ORBITS

We describe the procedure that we followed to determine periodic solutions for the systems Sprott A and NE9. This is not straightforward as the solutions are embedded in families of tori and have to pass through slow manifolds.

Finding (unstable) periodic solutions in dynamical systems is important for understanding and clarifying the mechanisms behind the emergence of strange attractors and the ensuing chaos. A whole branch of mathematics called *Periodic Orbit Theory* is devoted to this problem. There is a broad literature available in this area. See, for example[4] and the literature

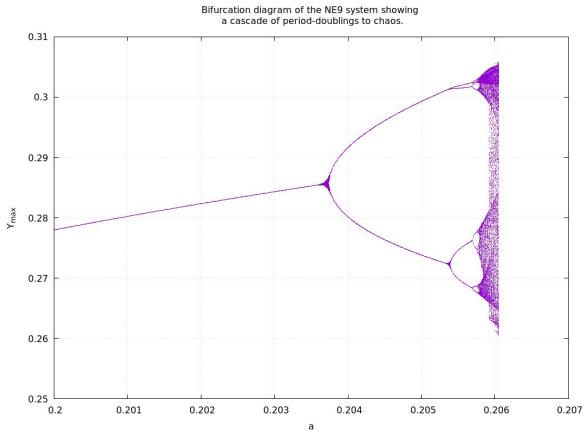

FIG. 21. The period doubling cascade in system NE9 starting at $a = 0.2$ leading to the chaotic set of fig. 20 at $a = 0.20601$.

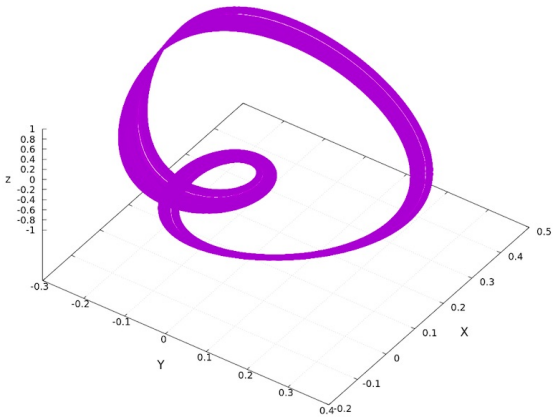

FIG. 22. Strange attractor from fig. 20 at $a = 0.20601$ arising from a cascade of period doublings, here displayed in 3-space.

therein. There is also a vast amount of literature and open source tools available on CAPD *Computer Assisted Proofs in Dynamics* and *interval arithmetics* to bridge the gap between what is numerically observed in simulations and what can actually be proved theoretically.

In this paper, a combination of techniques has been used to locate periodic orbits. First, the time-reversal symmetry is exploited to find R-symmetric periodic solutions. Theorem 4.1 in[9] is heavily used to reduce the dimensionality of the space of initial conditions that yield R-symmetric periodic solutions from 3 to 1. For completeness we reformulate here theorem 4.1 as stated in[9] for flows.

Theorem V.1

Let $o(x)$ be an orbit of the flow of an autonomous vector field with time-reversal symmetry R. Then:

- An orbit $o(x)$ is symmetric with respect to R if and only if $o(x)$ intersects $\mathrm{Fix}(R)$, in which case the orbit intersects $\mathrm{Fix}(R)$ in no more than two points and is fully

contained in $\mathrm{Fix}(R^2)$.

- An orbit $o(x)$ intersects $\mathrm{Fix}(R)$ in precisely two points if and only if the orbit is periodic (and not a fixed point) and symmetric with respect to R.

In the case of the sprottA system, $\mathrm{Fix}(R)$ is the $x-$axis. A direct consequence of the time-reversal symmetry is that R-symmetric periodic solutions of the sprottA system are Lyapunov stable and have all multipliers on the unit circle. The Lyapunov stability of the R-symmetric periodic solutions makes numerical detection feasible. Using theorem V.1, orbits starting on the x-axis are numerically integrated and the number of intersections with $\mathrm{Fix}(R)$ is monitored. All orbits that approximately intersect $\mathrm{Fix}(R)$ twice are labelled as 'potentially' periodic. This set of orbits is then used as first guess in continuation tools like Matcont[5] and Auto[6] to pinpoint their location exactly and compute their multipliers. Continuation even further with respect to the parameter a of the R-symmetric orbits as seeds yields branching point bifurcations with symmetry breaking yielding non-symmetric saddle periodic orbits. New unstable orbits are easily obtained from the R-symmetric ones through *Branching Point Bifurcations*. Most of the periodic orbits numerically found in this paper were obtained using this procedure. Note that the procedure is not exhaustive, in the sense that it does not guarantee the finding of all periodic solutions in the SprottA system. It is merely intended to be used as a 'light weight' and easy to implement technique to quickly find stable and unstable periodic orbits and investigate their involvement, if any, in the observed complexity and chaos in the SprottA and later on in the NE9 system. Not all unstable periodic solutions in the SprottA system branched off from an R-symmetric periodic solution. A second approach to find these saddles numerically was implemented by using the result from lemma I.4. The lemma guarantees a necessary condition for periodicity regardless of its stability character. The results of a numerical 3-d sweep of initial conditions yields potential candidates for periodic solutions that are then used as first guess in Matcont to generate the precise location and the multipliers accurately.

DISCUSSION AND CONCLUSIONS

1. As stated in[13], the presence of infinite families of tori for dissipative systems is a surprising phenomenon in systems Sprott A and NE9. It is analogous to the phenomenon of KAM tori near stable equilibrium of Hamiltonian systems. We have shown that for these dissipative systems it arises from the time reversal property of the systems.

2. Using rescaling of the differential equations, geometric singular perturbation theory adds valuable information on the qualitative and quantitative behaviour of the solutions near the origin of phase-space and near infinity.

3. It would be interesting to study the remaining 14 systems listed in[7] for the presence of time reversal, symmetry and invariant manifolds. It was shown in[1] that for $0 < a \ll 1$ system NE8 contains a family with canard behaviour but after some time the solutions tend to a stable periodic solution. System NE8 contains the z-axis as an invariant manifold but misses out on the time reversal with symmetry.

4. We found isolated tori and chaotic sets for the Sprott A and NE9 systems. It is an interesting open question how many more tori and chaotic sets exist in these systems.

ACKNOWLEDGMENTS

Earlier results in the litarature were kindly communicated to us by M. Messias. Suggestions for editorial improvements by the referees are gratefully acknowledged. .

Conflict of Interest

The authors have no conflicts of interest.

Data Availability Statement

The data that support the findings of this study are available from the corresponding author upon reasonable request.

[1] C. Abdulwahed and F. Verhulst. Recurrent canards producing relaxation oscillations. *Chaos*, 31, 2021. https://doi.org/10.1063/5.0040726.

[2] V.I. Arnold, V.V. Kozlov, and A.I. Neishadt. *Mathematical aspects of classical and celestial mechanics*. Dynamical Systems III (V.I. Arnlold, ed.). springer, 1988.

[3] M-C. Ciocci, A. Litvak-Hinenzon, and H.W. Broer. Survey on dissipative kam theory including quasi-periodic bifurcation theory. *Geometric Mechanics and Symmetry: the Peyresq Lectures*, 306:303–355, 2005.

[4] J. Crofts. *Efficient Method for Detection of Periodic Orbits in Chaotic Maps and Flows*. Ph.D. thesis, University of Leicester, 2007.

[5] Annick Dhooge, Willy Govaerts, Yu. Kuznetsov, W. Mestrom, A. Riet, and B. Sautois. Matcont and cl matcont: Continuation toolboxes in matlab. 07 2022.

[6] E. Doedel, A.R. Champneys, T.F. Fairgrieve, Yu.A. Kuznetsov, B. Sandstede, and X.J. Wang. *AUTO97: Continuation and bifurcation software for ordinary differential equations (with HomCont)*. Concordia University, Montreal, Canada, silver edition, 1997. User's Guide.

[7] S. Jafari, J.C. Sprott, and S. Golpayegani. Elementary quadratic chaotic flows with no equilibria. *Physics Letters A*, 377:699–702, 2013.

[8] M. Krupa and P. Szmolyan. Extending geometric singular perturbation theory to nonhyperbolic points - fold and canard points in two dimensions. *SIAM J. Math. Anal.*, 33:286–314, 2001.

[9] J.S.W. Lamb and J.A.G. Roberts. Time-reversal symmetry in dynamical systems: A survey. *Physica D*, 112:61, 1998.

[10] J. Laskar. Frequency analysis of a dynamical system. *Celestial Mechanics and Dynamical Astronomy*, 56:191–196, 1993.

[11] Peter De Maesschalck and Stephen Schecter. The entry-exit function and singular perturbation theory. *J. Diff. Eqs*, 260:6697–6715, 2016.

[12] M. Messias and A.C. Reinol. On the formation of hidden chaotic attractors and nested invariant tori in the sprott a system. *Nonlinear Dyn.*, 88:807–821, 2017.

[13] M. Messias and A.C. Reinol. On the existence of periodic orbits and kam tori in the sprott a system: a special case of the nosé-hoover oscillator. *Nonlinear Dyn.*, 92:1287–1297, 2018.

[14] J.A.G. Roberts and G.R.W. Quispel. Chaos and time-reversal symmetry. order and chaos in reversible dynamical systems. *Physics Reports*, 216:63–177, 1992.

[15] J.C. Sprott. Some simple chaotic flows. *Physical Review E*, 50:R647–R650, 1994.

[16] A.N. Tikhonov. Systems of differential equations containing a small parameter multiplying the derivative (in russian). *Math. Sb.*, 31 (73):575–586, 1952.

[17] Ferdinand Verhulst. *Nonlinear differential equations and dynamical systems*. Springer, New York, second edition, 2000.

[18] Ferdinand Verhulst. *Methods and applications of singular perturbations*. Springer, New York, 2005.